Chapter 8 Neural Network Implementation with Numerical Supervision

8.1. Purpose

This chapter serves to evaluate the feasibility of using neural networks trained with numerical supervision for damage quantification and qualification on an actual structure during operation. Industrial structures such as the Majuba Power Station FD and ID fans cannot be artificially damaged in order to do experimentally supervised neural network training due to the costs that will be involved in doing so. It would be ideal if the neural networks could be trained on numerically obtained features in order to be used on the actual structure, thus performing numerically supervised training.

With this in mind, the aim is to train neural networks solely on features obtained from FEM calculations using the updated FEM.

8.2. Introduction

Unlike in Chapter 7 where a lot of features were available to choose from, the only features available for network training are FRF energies and peak shifts obtained from the FEM. Although it is possible to obtain time signal estimations from the FEM, the accuracy of these estimations will be very doubtful due to the differences in excitation between the FaBCoM TeSt during operation and the FEM during testing. The reason why GMSFs cannot be used directly as features for neural network training, is the effect of modal density as described in Section 3.5.

In order to be able to use the neural networks trained on numerically obtained features for damage identification on the FaBCoM TeSt, several issues need to be taken into account:

- The FEM node or element locations, from which FRFs are to be calculated, should correspond to the FaBCoM TeSt sensor locations and orientations.
- The FEM result types should correspond to the FaBCoM TeSt measurement types. In other words, FEM FRFs should be calculated using strain or acceleration corresponding to the FaBCoM TeSt transducer measurements.
- Normalization of the experimentally obtained features to the numerical ones will probably be needed due to the differences between the two test procedures.
- The same frequency resolutions should be used for both numerical and experimental features.

8.3. FEM Testing Procedure

Figure 8-1 shows the setup for the FEM FRF calculations with the measurement locations corresponding to those of the experimental setup as well as the blade numbers.

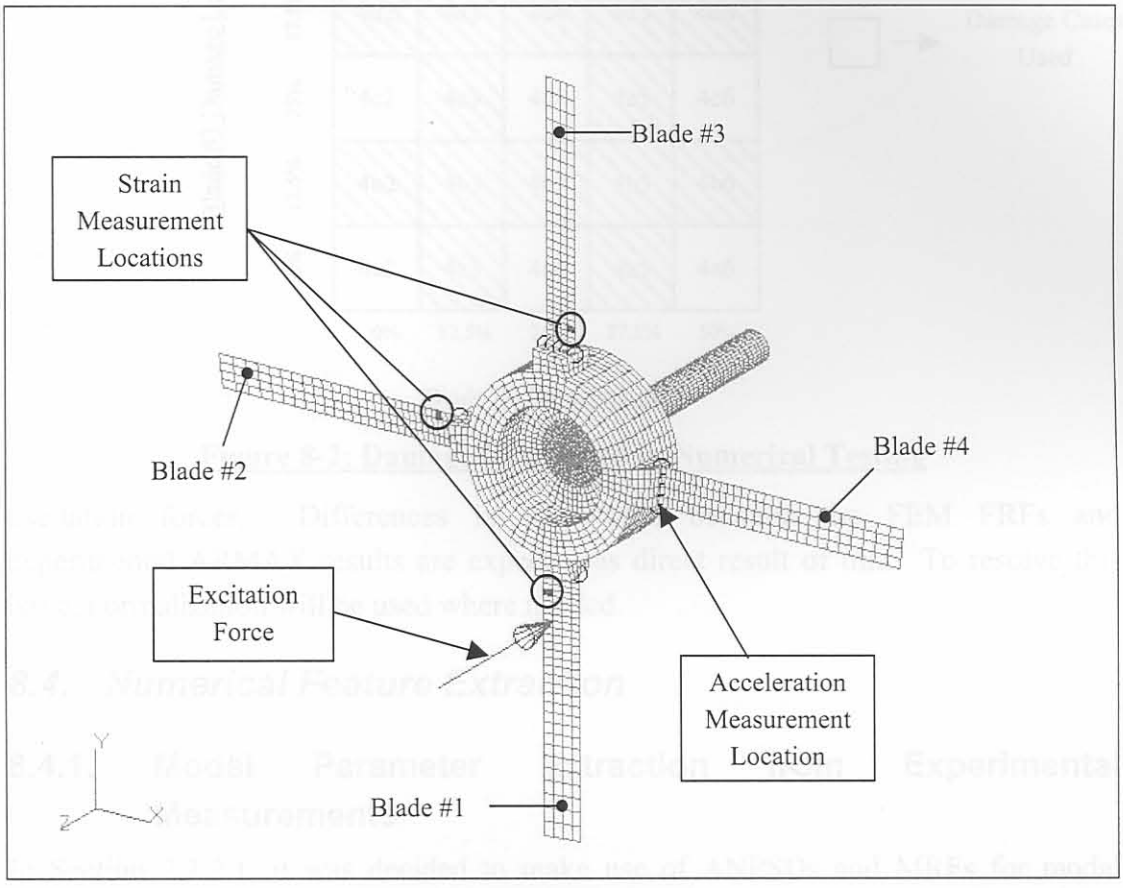

Figure 8-1: FEM Test Setup

The FEM can only be tested for blade root damage increments of 25%. This is due to the element mesh resolution of the blades as described in Section 2.3. As in Chapter 6, damage was simulated at blade #3 and blade #4. The same procedure was followed as depicted in Figure 6-3 except for the damage increments being 25% and not 12.5%. Comparing to Figure 6-1, Figure 8-2 gives the damage cases used for FEM testing. Damage was simulated in the FEM by deleting appropriate MPCs. This is similar to the nodal dissociation method used by Smit [45] for crack modelling.

The point of excitation as shown in Figure 8-1 was chosen to be the same as that used in the EMA for the reason of allowing torsional, sideways and normal excitation of the structure. A constant excitation force of 1 N was chosen over an excitation bandwidth of 2000 Hz at 2.5 Hz intervals. Thus a single white noise input force is simulated corresponding to turbulent forces experienced by operational wind turbines ([2]). In the FaBCoM TeSt however, the force inputs are more complex as they are distributed forces and comprise of turbulent force inputs as well as rotational excitation by the electric motor, blade pass frequency excitation and other operational

Figure 8-2: Damage Cases used in Numerical Testing

excitation forces. Differences in amplitudes between the FEM FRFs and experimental ARMAX results are expected as direct result of this. To resolve this issue, normalization will be used where needed.

8.4. Numerical Feature Extraction

8.4.1. Modal Parameter Extraction from Experimental Measurements

In Section 7.2.2.1, it was decided to make use of ANPSDs and MRFs for modal parameter extraction instead of ARMAX modelling due to computational costs. However, ANPSDs and MRFs were found to be much less accurate then ARMAX models results. Also, once an ARMAX model is estimated for a time signal, it is very easy to obtain modal frequencies for that model. Smit [45] used 48^{th} order ARMAX models as he found this to be sufficient for datasets with sampling frequencies of 5120 Hz and a bandwidth of 2000 Hz. As the same experimental setup was used in this dissertation as in Smit's, it was decided to use the same order ARMAX models. The software used to calculate the ARMAX models was the System Identification Toolbox Version 5 for Matlab.

8.4.2. Peak Frequency Normalization

As described in Section 5.1.2, not all the natural frequencies of the FEM are equal to that of the FaBCoM TeSt. For this reason, FRF peak normalization in terms of frequencies needs to be done as shown in Figure 8-3 for EMS #4. For frequency normalization, use was made of factorisation. The frequency ranges used for FEM FRF peak identification were chosen to be from 5 Hz below the modal frequencies for 50% damage of blades #3 and #4, and to 5 Hz above the modal frequencies for the

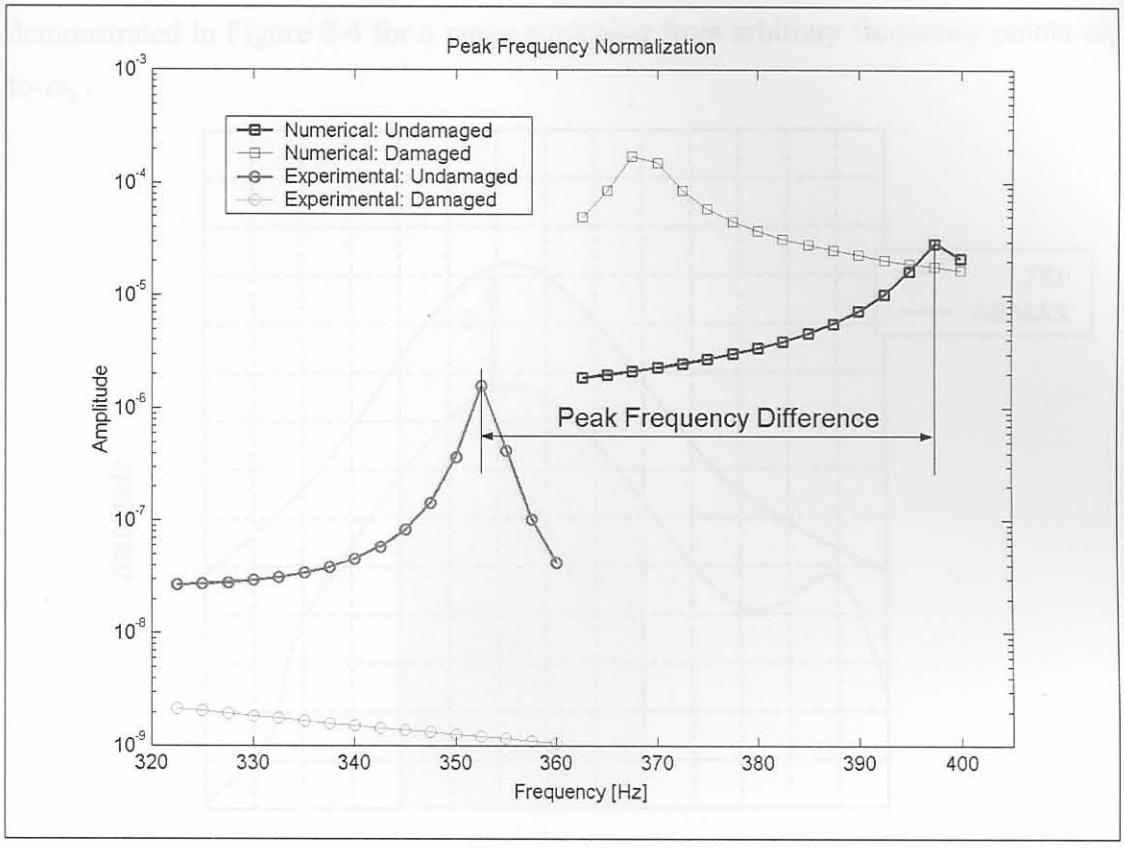

Figure 8-3: Peak Frequencies for EMS #4

undamaged case. For experimental peak identification, the top frequency limits were chosen to be 5 Hz above the experimental modal frequencies for the undamaged case. The lower ranges were determined by the ranges used in the corresponding FEM in order to obtain the same number of curve points for the respective experimental and FEM ranges. To explain this more mathematically, let the FEM FRF peak frequency range for a specific peak stretch from a lower limit ω_1 to a higher limit ω_2. If the frequency range for the corresponding experimental peak stretches from a lower limit ω_3 to ω_4, then the limit differences are equal as given by Equation (8-1):

$$\omega_2 - \omega_1 = \omega_4 - \omega_3 \qquad (8\text{-}1)$$

8.4.3. Energy Normalization

As discussed in Section 8.3, differences in amplitudes between the FEM FRFs and experimental ARMAX results are expected. This is also confirmed in Figure 8-3. Energy normalization was performed only after peak normalization was performed.

The first step of normalization of numerically obtained features to experimental features is based on the assumption that for a certain frequency range, the amplitudes of a numerical FRF will differ to that of the corresponding experimental ARMAX model FRF amplitudes by a constant over that range. This is graphically

demonstrated in Figure 8-4 for a range stretching from arbitrary frequency points ω_1 to ω_2.

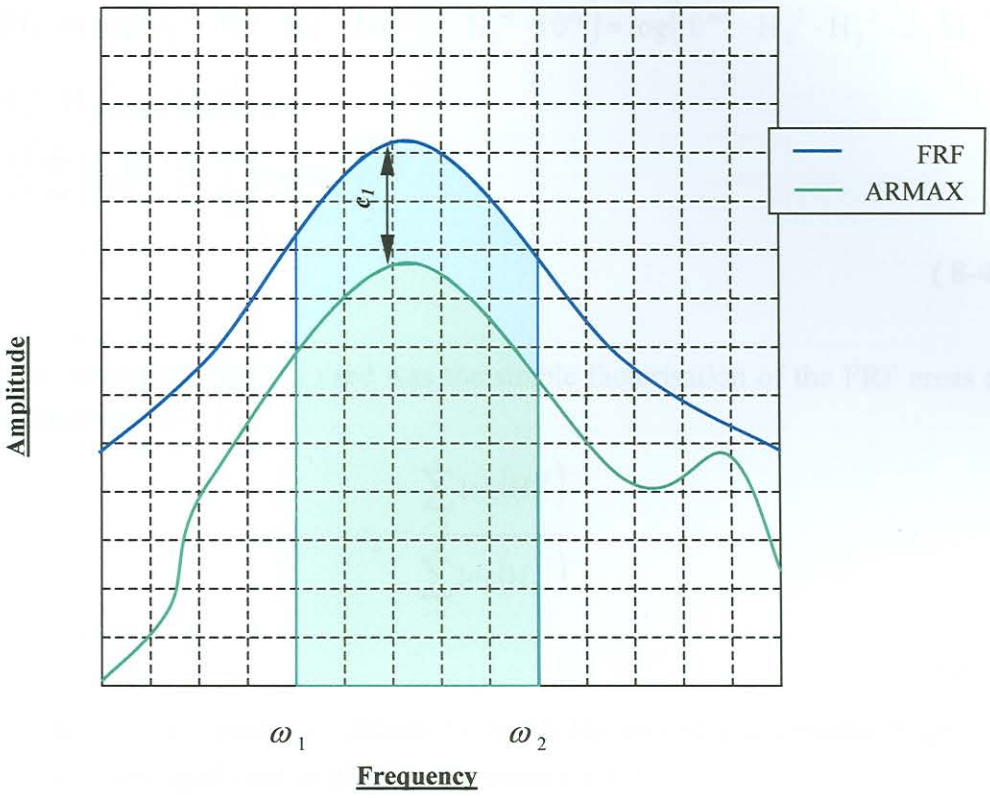

Figure 8-4: Frequency Response Function Offset Assumption

To express this mathematically, let $H_1(\omega)$ and $H_2(\omega)$ be an experimental ARMAX model FRF and a numerical FRF respectively at an arbitrary frequency within a frequency range stretching from ω_1 to ω_2, so that

$$\log(H_1) = \log(H_2) + c_1$$
$$\therefore \log(H_1) - \log(H_2) = c_1$$
$$\therefore \log\left(\frac{H_1}{H_2}\right) = c_1$$
$$\Rightarrow \frac{H_1}{H_2} = 10^{c_1}$$

(8-2)

For n discrete points over this frequency range, the area underneath the curve H_1 over the range is given by

$$\sum_{i=1}^{n} \log\left(H_1{}^{i}\right) = \log\left(H_1{}^{1}\right) + \log\left(H_1{}^{2}\right) + \ldots + \log\left(H_1{}^{n}\right) = \log\left(H_1{}^{1} \cdot H_1{}^{2} \cdot \ldots \cdot H_1{}^{n}\right)$$

(8-3)

Equation (8-3) can also be written for H_2.

Using Equation (8-2) and assuming c_1 remains constant over the specified range, Equation (8-4) is obtained:

$$\sum_{i=1}^{n}\log\left(H_1^{\,i}\right)=\log\left(H_2^{\,1}\cdot 10^{c_1}\cdot H_2^{\,2}\cdot 10^{c_1}\cdot\ldots\cdot H_2^{\,n}\cdot 10^{c_1}\right)=\log\left(10^{nc_1}\cdot H_2^{\,1}\cdot H_2^{\,2}\cdot\ldots\cdot H_2^{\,n}\right)$$

$$=\log\left(H_2^{\,1}\cdot H_2^{\,2}\cdot\ldots\cdot H_2^{\,n}\right)+nc_1$$

$$\therefore c_1=\frac{1}{n}\left[\sum_{i=1}^{n}\log\left(H_1^{\,i}\right)-\sum_{i=1}^{n}\log\left(H_2^{\,i}\right)\right] \qquad (8\text{-}4)$$

The second normalization step used was the simple factorisation of the FRF areas as given in Equation (8-5):

$$c_2=\frac{\sum_{i=1}^{n}\log\left(H_1^{\,i}\right)}{\sum_{i=1}^{n}\log\left(H_2^{\,i}\right)} \qquad (8\text{-}5)$$

The frequency ranges used was chosen to be 10 Hz around each modal frequency (ω_m) for the undamaged case as given in Equation (8-6):

$$\omega_1=\omega_m-5\text{ Hz}\ \text{ and }\ \omega_2=\omega_m+5\text{ Hz} \qquad (8\text{-}6)$$

To obtain the final normalized energies, these two normalization steps are combined as given for a frequency range by Equation (8-7):

$$\text{Normalized Energy}=\frac{1}{2}\left[\left(\sum_{i=1}^{n}\log\left(H_2^{\,i}\right)+nc_1\right)+\left(c_2\times\sum_{i=1}^{n}\log\left(H_2^{\,i}\right)\right)\right] \qquad (8\text{-}7)$$

With the frequency resolution used (as described in Section 8.3) together with the frequency range definition given by Equation (8-6), it means that the number of discrete points in these ranges, n, will be equal to five.

8.5. Neural Network Training

Several neural networks were trained with different goals in mind namely global damage quantification, global damage qualification, sensor position identification, blade #3 damage quantification and blade #4 damage quantification. For each of these, several networks of different complexities in terms of network architecture were trained in order to make use of neural network committees as suggested by Marwala [33]. In this way, the unique characteristics of the different networks were

combined to yield the best results. The network architectures used in each network committee are listed in Table 8-1.

Table 8-1: Network Committees Network Architectures

	Committee	Global Blade Damage			
	Network Number	4	5	6	7
	Dimensions	12x1	11x1	10x1	9x1
Transfer Function	Layer 1	TSTF	TSTF	TSTF	TSTF
	Layer 2	LTF	LTF	LTF	LTF
	Layer 3	-	-	-	-
	Layer 4	-	-	-	-
	Committee	Multiple Blade Damage			
	Network Number	1	15	16	17
	Dimensions	6x4	12x4	12x6x4	12x10x4
Transfer Function	Layer 1	TSTF	TSTF	TSTF	TSTF
	Layer 2	LTF	LTF	TSTF	TSTF
	Layer 3	-	-	LTF	LTF
	Layer 4	-	-	-	-
	Committee	Blade Identification			
	Network Number	2	3	8	9
	Dimensions	6x8x1	6x8x4x1	12x1	10x1
Transfer Function	Layer 1	TSTF	TSTF	TSTF	TSTF
	Layer 2	TSTF	TSTF	LTF	LTF
	Layer 3	LTF	TSTF	-	-
	Layer 4	-	LTF	-	-
	Committee	Blade #3 Damage			
	Network Number	18	19	20	21
	Dimensions	12x6x2x1	12x1	12x6x1	12x6x2x1
Transfer Function	Layer 1	TSTF	TSTF	TSTF	TSTF
	Layer 2	TSTF	LTF	TSTF	TSTF
	Layer 3	TSTF	-	LTF	TSTF
	Layer 4	LTF	-	-	LTF
	Committee	Blade #4 Damage			
	Network Number	10	12	13	14
	Dimensions	12x1	12x6x2x1	6x6x2x1	6x8x2x1
Transfer Function	Layer 1	TSTF	TSTF	TSTF	TSTF
	Layer 2	LTF	TSTF	TSTF	TSTF
	Layer 3	-	TSTF	TSTF	TSTF
	Layer 4	-	LTF	LTF	LTF

Three sets of training data were used, containing the features extracted for all of the nine damage cases from the FEM strain FRFs of blades #1, #2 and #3 respectively as well as from the rotational FEM acceleration FRFs at the root of blade #4. Each dataset consisted of the a total of six features namely the frequency shifts of EMSs #4

and #6 as well as the energies of EMS #X for both the strain signal from the particular blade for the training set and the rotational acceleration signal.

8.6. Neural Network Testing

All the network committees were tested using nine additional experimental data sets for each of testing sets #1, #2 and #3 as listed in Table 8-2. The results yielded are presented in Figure 8-5 to Figure 8-9 with the damage cases numbered sequentially according to dataset number. Each testing set number indicates which blade's strain signal features were used for that dataset. As in Chapter 7, the results yielded were averaged to obtain more representative results.

Table 8-2: Training and Testing Sample Numbering

	Sample #		
Damage Case	**Testing Set #1**	**Testing Set #2**	**Testing Set #3**
4a2	1	10	19
4c2	2	11	20
4e2	3	12	21
4a4	4	13	22
4c4	5	14	23
4e4	6	15	24
4a6	7	16	25
4c6	8	17	26
4e6	9	18	27

First, the use of a neural network committee for global damage quantification was explored. Rather good results are obtained as shown in Figure 8-5. This network committee is a bit conservative with regards to global blade damage detection when blade #4 is undamaged, as a higher damage level is detected than what is actually present. The results are roughly similar for all three training sets.

Networks were then trained for quantifying damage for all four blades simultaneously. Figure 8-6 shows the network committee results where it can be seen that very good results are obtained for blade #3 damage detection while less well results are obtained for blade #4.

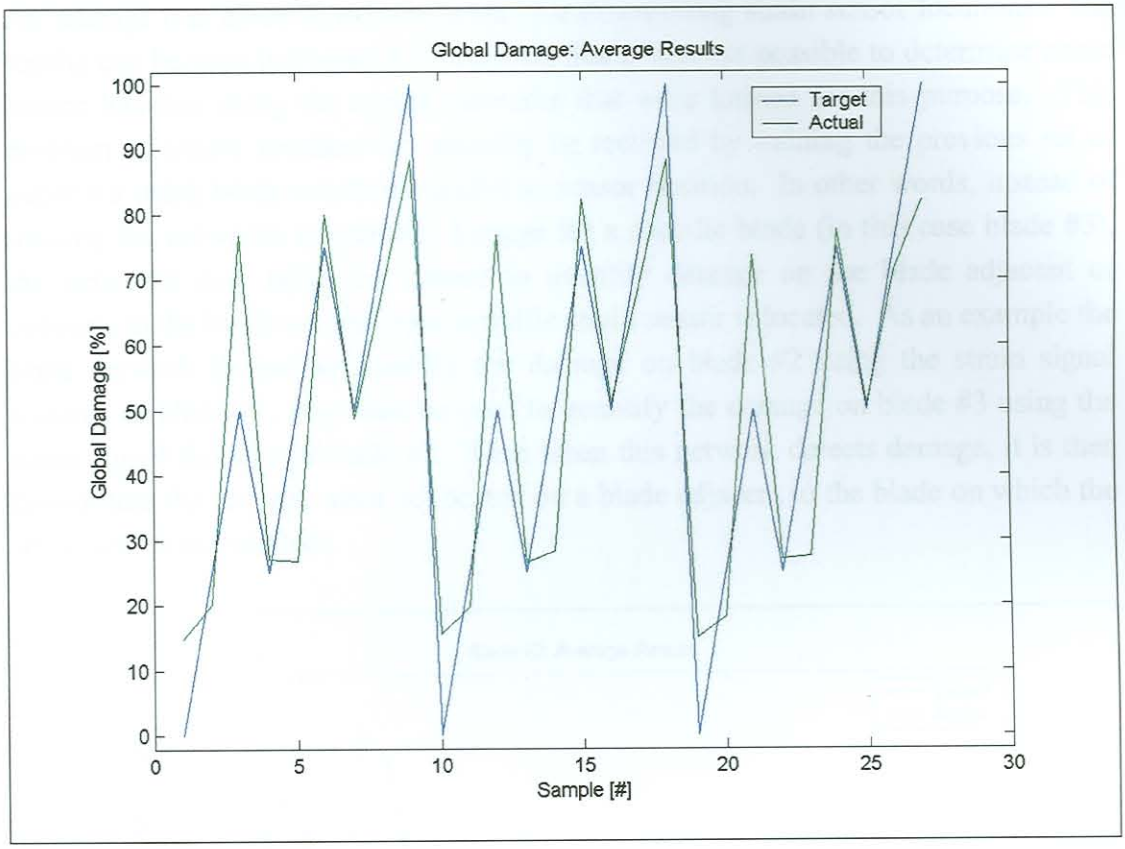

Figure 8-5: Global Blade Damage Detection Network Committee Results

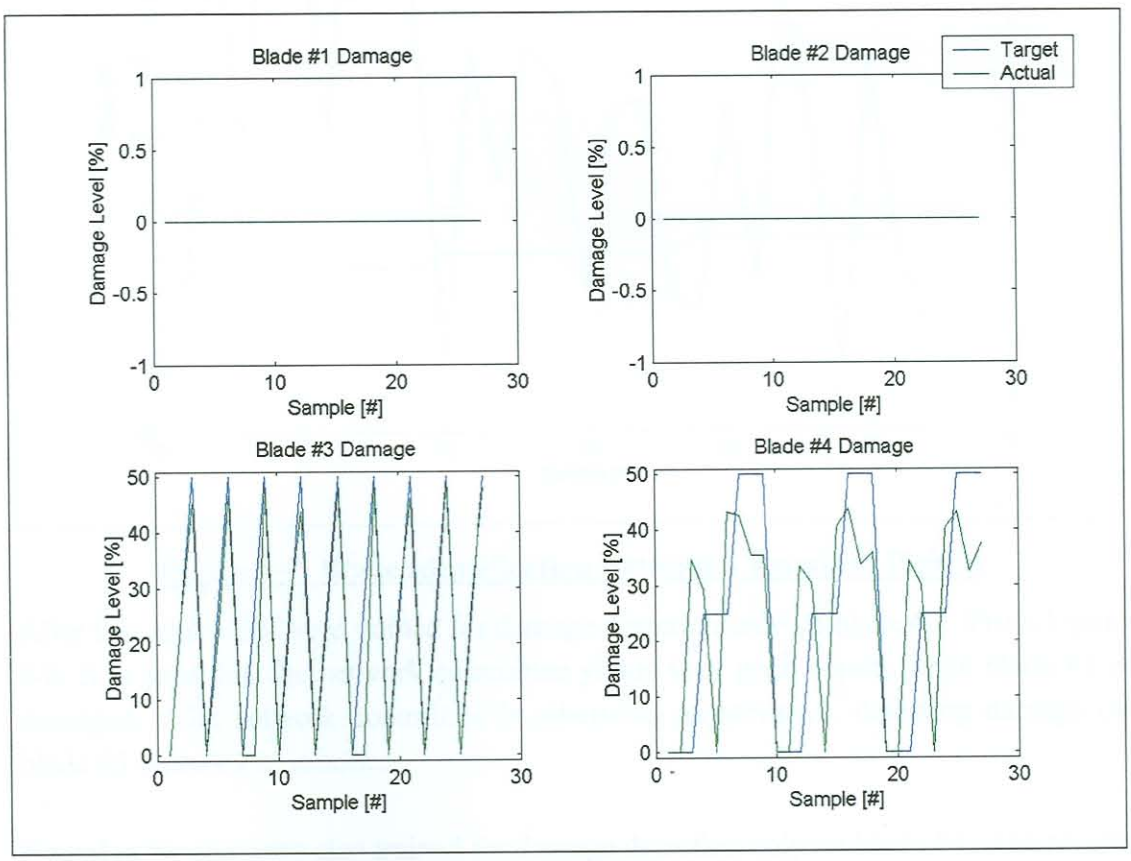

Figure 8-6: Multiple Blade Damage Detection Network Committee Results

An attempt was made to train networks for determining strain sensor locations. The results can be seen in Figure 8-7, showing that it was not possible to determine strain sensor location using the neural networks that were trained for this purpose. This problem of sensor location can possibly be rectified by training the previous set of networks using blade numbers relative to sensor position. In other words, instead of training the networks to quantify damage for a specific blade (in this case blade #3), the networks may rather be trained to quantify damage on the blade adjacent or opposite to the blade on which the specific strain sensor is located. As an example the same network trained to quantify the damage on blade #2 using the strain signal features of blade #1, may then be used to quantify the damage on blade #3 using the strain signal features of blade #2. Thus when this network detects damage, it is then known that the damage must be located on a blade adjacent to the blade on which the strain sensor is installed.

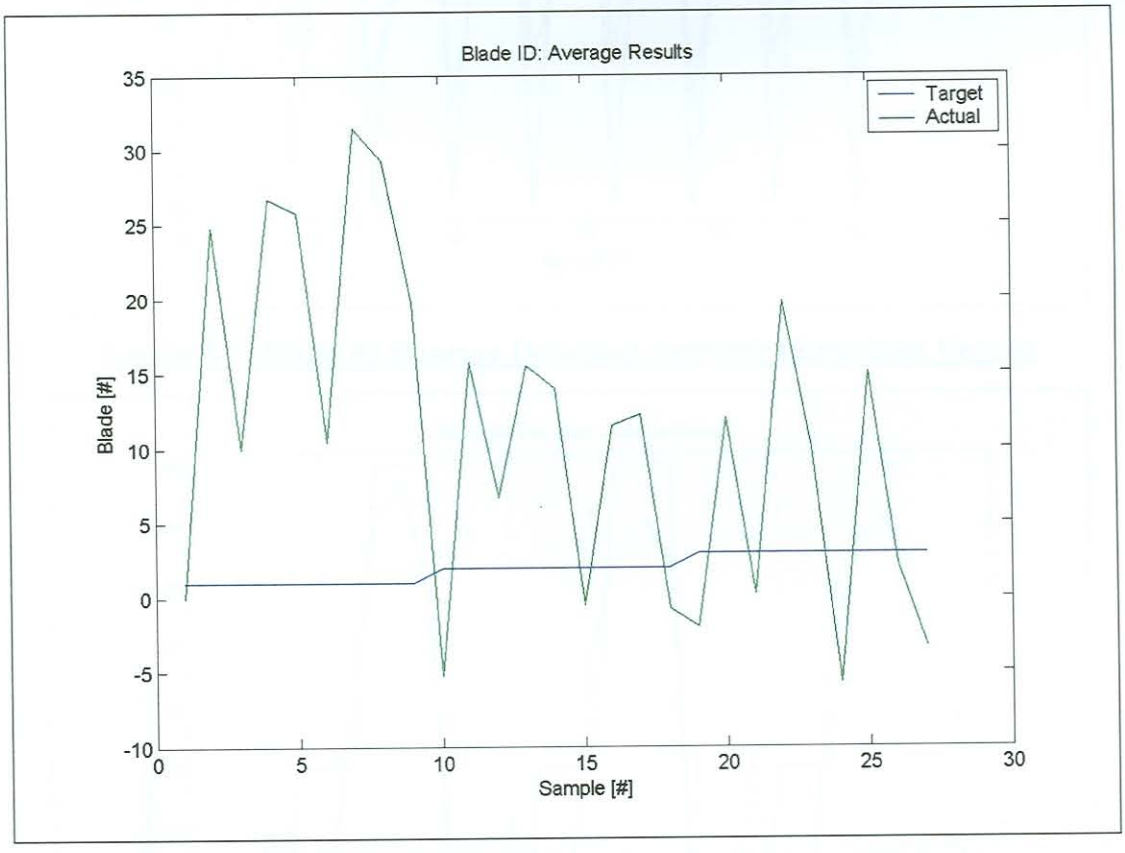

Figure 8-7: Blade Identification Network Committee Results

After this, networks were trained for damage detection only on blade #3. From Figure 8-8, it is seen that the network committee yields very good results when blade #3 is damaged. The network committee is otherwise conservative, detecting damage on blade #3 when there is none.

Neural networks were also trained for damage detection only on blade #4. The results of the network committee are shown in Figure 8-9. Relatively good results are

obtained for an undamaged blade #4 with blade #3 damage below 50%. Blade #3 damage has a large effect on the results at blade #4 damage levels of 25% and below. Overall, the results are not very accurate but are still indicative of blade #4 damage.

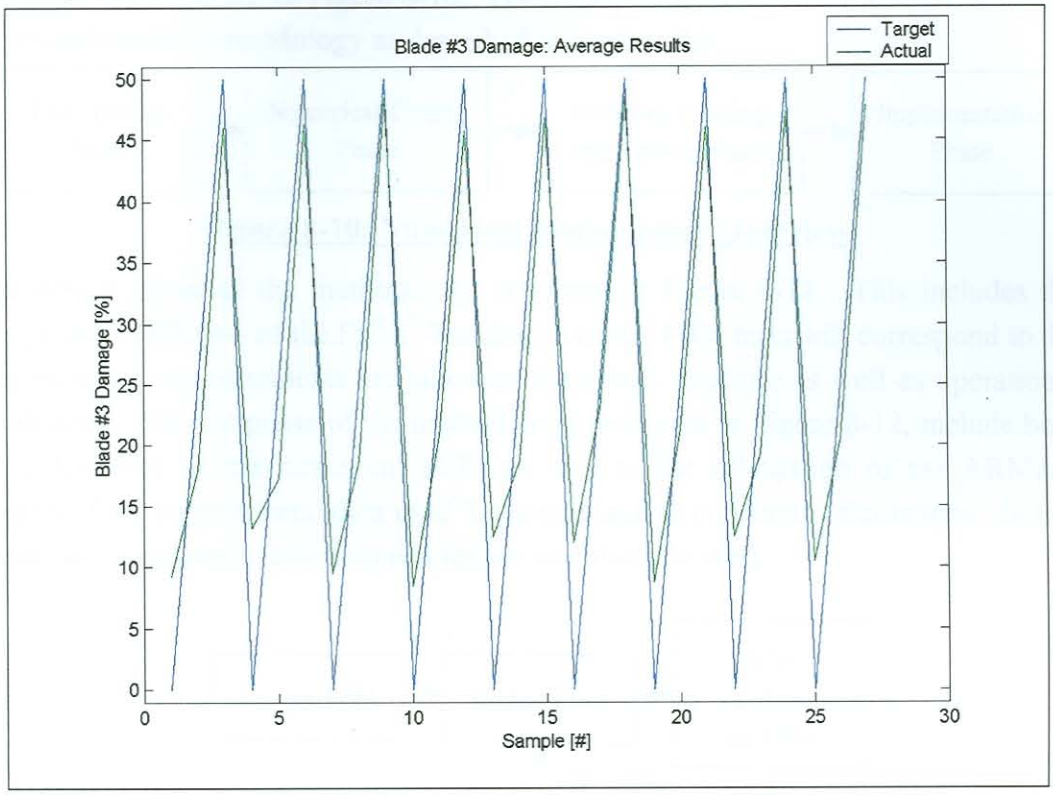

Figure 8-8: Blade #3 Damage Detection Network Committee Results

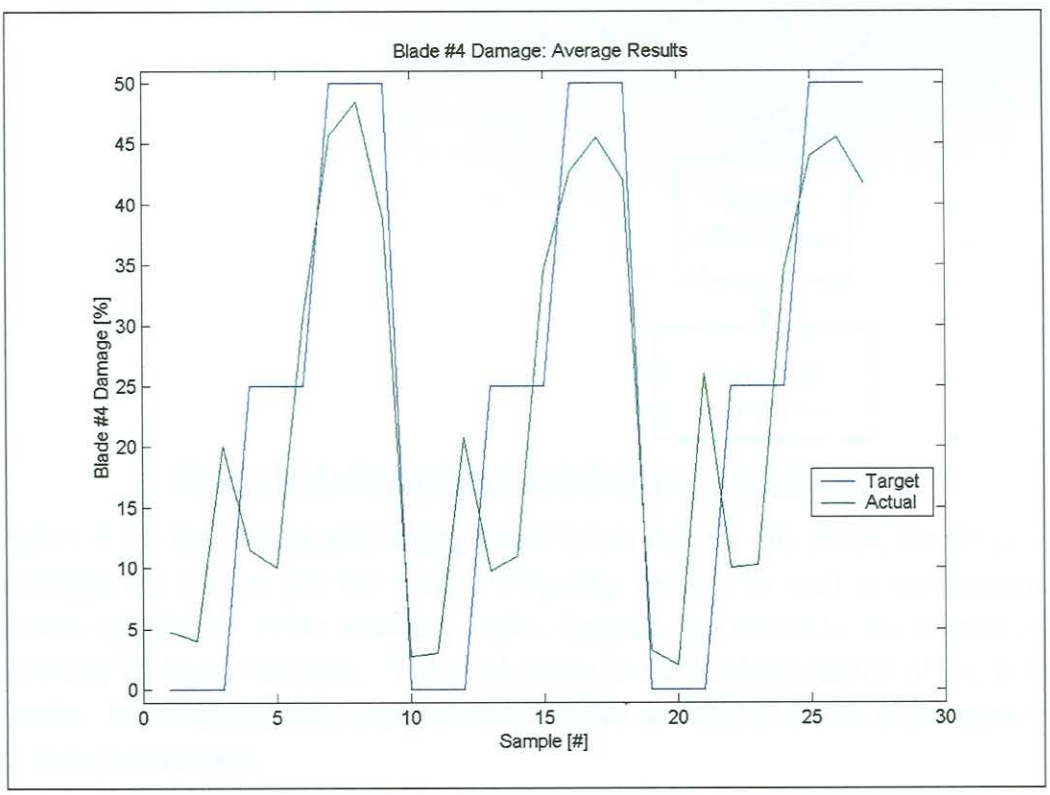

Figure 8-9: Blade #4 Damage Detection Network Committee Results

8.7. Numerical Methodology Summary

An overview of the numerically supervised neural network damage detection methodology is shown in Figure 8-10. The methodology phases are similar to that of the experimental methodology as described in Section 7.6.

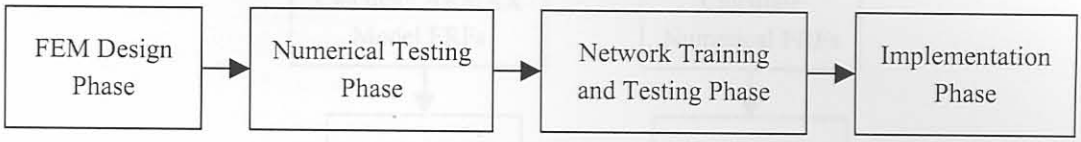

Figure 8-10: Numerical Methodology Overview

The design phase of the methodology is shown in Figure 8-11. This includes the design and validation of the FEM. The design of the FEM tests will correspond to the way in which measurements are taken on the actual structure as well as operational conditions. The test phase of the methodology as shown in Figure 8-12, include both the calculation of the numerical FRFs as well as the calculation of the ARMAX models of the experimental data used for normalization constants calculations. In this phase, the necessary modal frequencies are calculated as well.

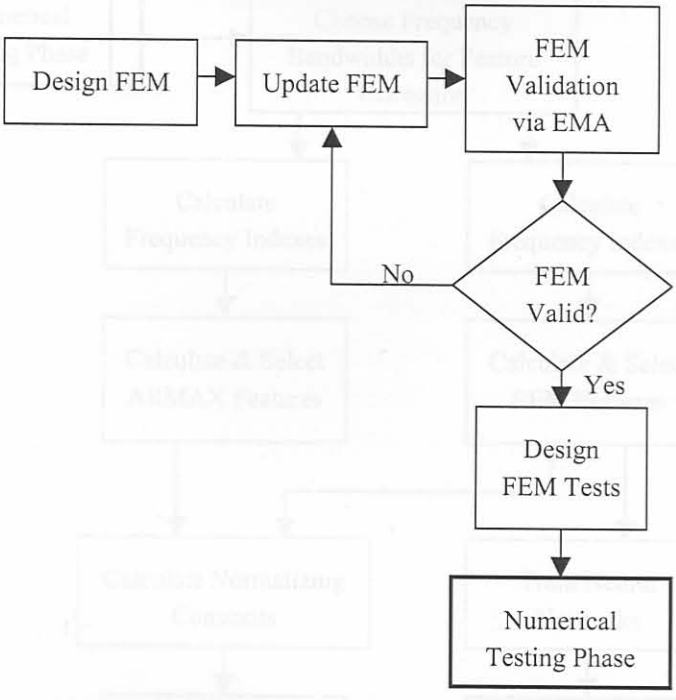

Figure 8-11: Numerical Methodology Design Phase

In Figure 8-13, the training and testing phase is laid out. In this phase, the frequency bandwidths are chosen and the feature frequency indexes as well as normalization constants calculated. After selecting usable features, the networks are trained after performing PCAs on the data. The final phase is the implementation of the neural networks. In this phase, only experimental features are used as inputs to the networks after being normalized.

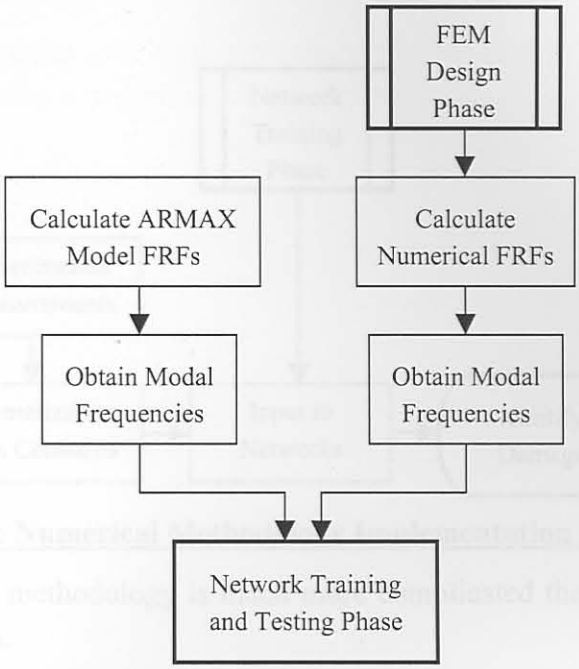

Figure 8-12: Numerical Methodology Test Phase

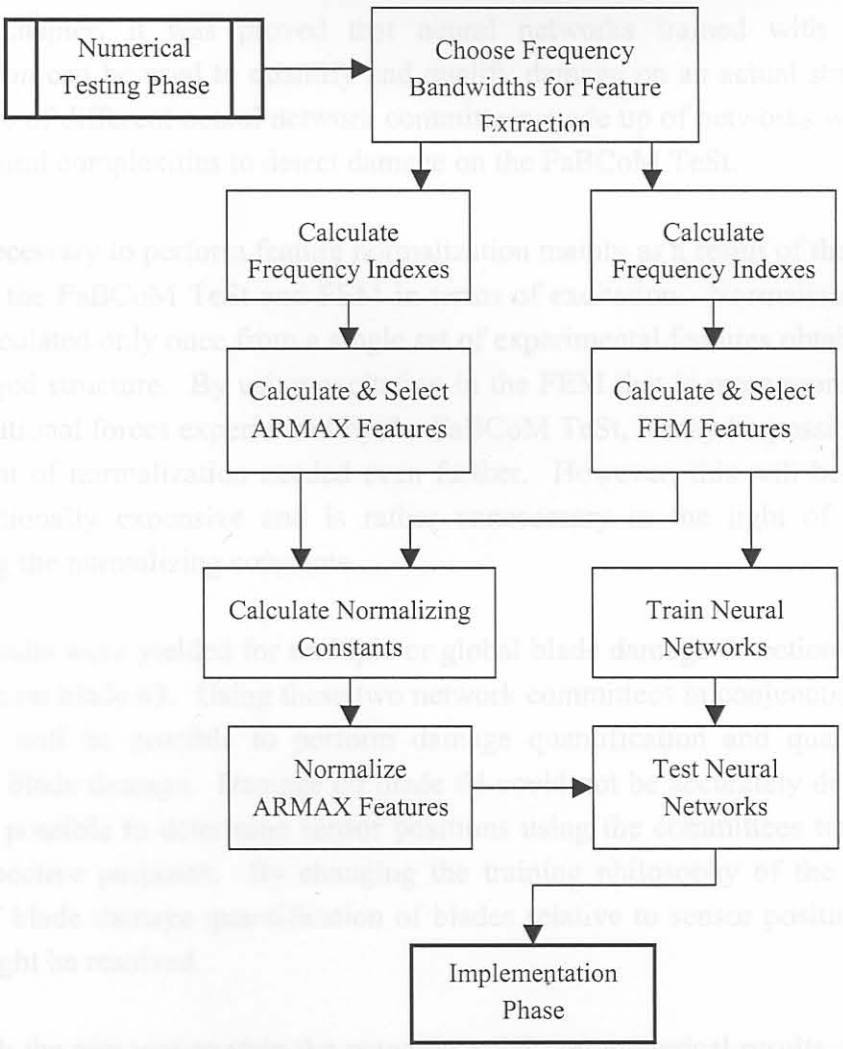

Figure 8-13: Numerical Methodology Training and Testing Phase

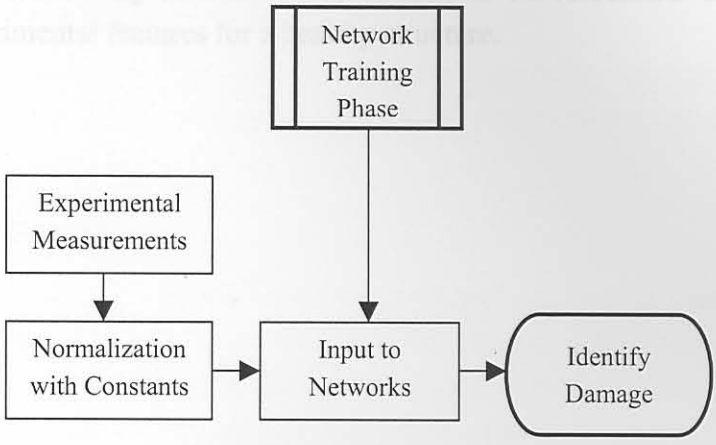

Figure 8-14: Numerical Methodology Implementation Phase

It is very clear that the methodology is much more complicated than that of the one presented in Section 7.6.

8.8. Conclusion

In this chapter, it was proved that neural networks trained with numerically supervision can be used to quantify and qualify damage on an actual structure. Use was made of different neural network committees made up of networks with different architectural complexities to detect damage on the FaBCoM TeSt.

It was necessary to perform feature normalization mainly as a result of the differences between the FaBCoM TeSt and FEM in terms of excitation. Normalizing constants were calculated only once from a single set of experimental features obtained from an undamaged structure. By using excitation in the FEM that is more representative of the operational forces experienced by the FaBCoM TeSt, it may be possible to reduce the extent of normalization needed even further. However, this will be much more computationally expensive and is rather unnecessary in the light of the ease of obtaining the normalizing constants.

Good results were yielded for multiple or global blade damage detection and damage detection on blade #3. Using these two network committees in conjunction with each other, it will be possible to perform damage quantification and qualification for multiple blade damage. Damage on blade #4 could not be accurately detected and it was not possible to determine sensor positions using the committees trained for the two respective purposes. By changing the training philosophy of the networks in terms of blade damage quantification of blades relative to sensor position, the latter issue might be resolved.

Although the aim was to train the networks solely on numerical results, use was still made of a set of experimental features for calculation of normalization constants.

However, these normalizing constants only needed to be calculated once using a single set of experimental features for a healthy structure.